

Application of the point-like contact model: Resistance Oscillations of the Domain Wall in Magnetic Nanowires and Junctions due to Mean Free Path Effects

Artur Useinov

*International College of Semiconductor Technology, National Yang Ming Chiao Tung University
1001 Ta Hsueh Rd, Hsinchu, 30010, Taiwan R.O.C.
artu@nycu.edu.tw*

Received 20 October 2021
Accepted 14 December 2021

This work is focused on determining the electrical resistance, which induced by single domain wall in magnetic nanowire with a negligible defect. The provided model covers a wide range of nanowire's diameters. The obtained result demonstrates a few orders rapid reduction of the domain wall resistance accompanied by its possible deviations *versus* the diameter growth ranging from 1.2 nm to 15.2 nm. The origin of these deviations, which are also identified as oscillations, is referred to the non-uniform electron scattering on the domain wall due to the intermixing electron scattering conditions: ballistic for one spin channel and quasi-ballistic for other one with opposite spin direction. It may happen when the domain wall width by value is approximately in between two lengths: a mean free path with the spin down and spin up. The indirect evidence of this finding is also coming from the fact that homogeneous nanowires shows the most valuable domain wall resistance oscillations by magnitude rather than segmented magnetic nanowires. In addition to the approach, where DW width is constant, the other reasonable model is used when the domain wall can be constrained for some conditions. The same results are valid for magnetic junctions with domain wall. Finally, resistance simulation in the diffusive range, when a diameter of the nanowire (or point-like junction) is larger than any of spin resolved mean free path of electrons, successfully follows experimental data for the single and double domain wall resistances available in literature.

Keywords: Nanomagnetism, magnetic domain wall, resistance, ballistic magnetoresistance, nanowires.

1. Introduction

The control of magnetic domain wall (DW) motion and resistive states are key points for electronic applications. For example DW can be utilized for a computational logic¹, energy-effective memristor², magnetic synapse for neural network³, working cell of the magnetic DW racetrack memory⁴, *etc.* Natural lattice defects, artificially created interfaces between different segments in magnetic nanowires (NWs)⁵; ⁶ as well as geometrical modulations⁷ are

potential centers for a DW trapping. Numerous theoretical and experimental works focused on the investigation of the dynamical motion of the single DW⁸; ⁹ and its resistance impact¹⁰; ¹¹; ¹²; ¹³. One of these theoretical works generated a model of the total resistivity of the thin ferromagnetic films showing that both transversely and longitudinally oriented DWs are additional source of the resistivity¹⁰. In contrast, focusing on the ferromagnetic wires with DWs, another work showed that

resistivity can be decreased by the reason of electron decoherence due to DW nucleation¹¹. In addition, application of the semiclassical model^{14, 15} of the point contact (PC) allows to estimate giant ballistic magnetoresistance (BMR)¹⁶ as well as single DW resistance in magnetic nanojunctions and nanowires, where the resistance due to electron scattering on the DW only increases.

The novel specific DW state, which is almost independent of the material parameters and located in a ferromagnet within a nanoconstriction, was discovered by Bruno¹⁷. The width of this DW type is conjugated with the dimension of the constriction and can be much smaller in contrast to the well-known Bloch- and Néel- DW types. Bruno made the numerical estimations of the DW width and energy, showing the evidence of the giant BMR in nanoscale PCs. Furthermore, after Bruno's predictions and further model development by Yan *et al.*⁹, experimental detection of the novel Bloch-point DW was obtained by Da Col *et al.*¹⁸ in a cylindrical magnetic NWs. It was claimed that Bloch-point DW is the zero-mass nanomagnetic object with topologically protected state and transverse magnetic geometry, having a unique dynamic properties. The transverse ordering of the magnetizations (along NW) is more preferred magnetic state in NWs with diameter $d_0 < 250$ nm rather than a vortex state, observed in the work¹⁹ for the case $d_0 > 250$ nm, where magnetization are curling around the wire axis. The prevention of the vortex states is kept due to domination of the exchange energy against dipolar and anisotropy energies^{18; 20}. When the lateral dimension of the NW achieves 40 nm, or less, the physics of the electron transport is changed due to quantum confinement. The goal of present work is calculation of the DW resistance and its behavior at the confined geometry, assuming that magnetizations (M) are oriented along magnetic NW and DW is characterized as linear slope of M projections. The dimensional factor becomes dominated, since mean free paths (MFP) of the spin-resolved carriers are now comparable with DW width. For simplicity, the possible NW anisotropy change is omitted from consideration.

2. Theoretical Model

The main benefit of the present model is the adaptation of the PC model¹⁵ for DW resistance (ΔR) simulation in magnetic NWs within an approach

of the tail-removed linear DW approach, Fig.1a. Whatever the DW's 3D magnetization direction behavior is, the most important for an electron transport is its projection on the axis of the transport direction z . For simplicity, the red solid line is adjusted as such projection for the present model and, at the same time, the red curve is a linear potential energy profile which spin-down electron has along z . Spin-up electron has a mirror reflected potential in relation to z axis due to exchange energy, according the Stoner model. To explain ΔR behavior in NW, it is assumed, that NW contains a small idealized defect, which is considered as PC, and diameters of NW and PC are almost the same values: $d_0 \approx d$, that make DW-induced potential energy profile a valuable contributor to the PC's resistance in addition to other source - the resistance related with PC's geometrical constriction due to MFP effects²¹. The same model will work for ΔR coming from DW located nearby PC in magnetic junction without an existence of NW (at this case, there is only d , and d_0 is out of consideration).

The possible most exact dependences of the DW projections are presented in Fig.1a: $M_Z(z) = M_S \times \tanh(z/t_{DW})$ and $M_Z(z) = M_S(2/\pi) \arcsin[\tanh(2z/t_{DW})]$ as green dash-dot and orange dashed curves, respectively. They are not considered here for simulations due to complicated solution of the Schrödinger equation. In present model both these profiles are exchanged on the linear slope profile $M_Z(z) = M_S \times z/t_{DW}$ shown by red solid curve. In terms of electron potential energy it corresponds to $U(z) \approx E_{ex}z/t_{DW}$, where E_{ex} is exchange energy in ferromagnet. Furthermore, the condition of the Bruno's model¹⁷, where the DW width (t_{DW}) strongly correlates with d at the restricted geometry $t_{DW} \approx d$ is important. The DW width becomes constant when d_0 increases and overpass some dimensional threshold t_0 , Fig.1b, and the tilting of the projection profile increases at this case.

In terms of applications, the problem is actual for a system with large amount of magnetic NWs (PCs) having distribution by d_0 (d), *i.e.* the set of the NWs (PCs) with varies d_0 (d), or for a single cone-like NW, which has a periodically located defects. The present model is applicable for homogeneous as well as for segmented magnetic NWs, and the DW is pinned in the center of the PC, or on the interface between segments, respectively. In real cases, DW center can stuck nearby defect location

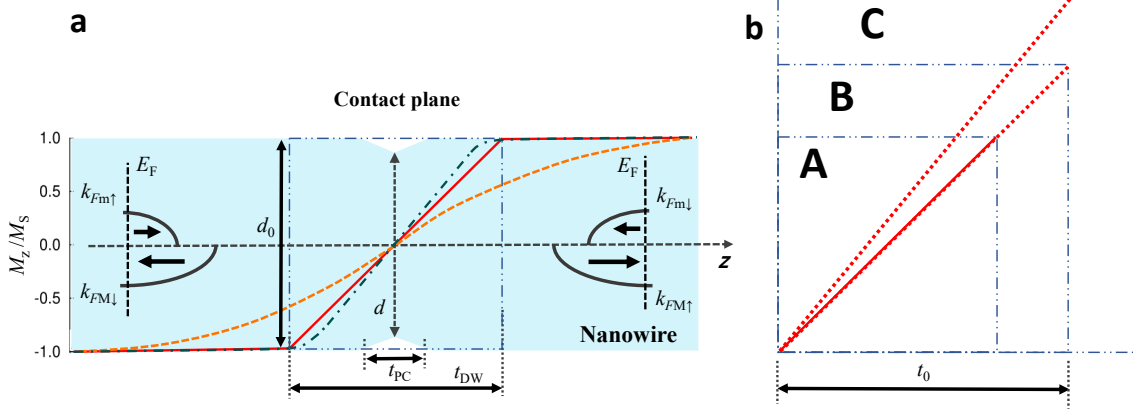


Fig. 1. Magnetization projections of DWs in nanowire: **a** The geometrically constrained DW with magnetic tail as the most relevant model of the constrained state is shown as green dash-dot curve; The constrained ($t_{\text{DW}} = d$) tail-removed linear projection as a simplified DW approach of the present model is shown as red solid line; And alternative magnetic DW profile is shown as orange dashed line. The left and right sketches show the majority and minority electron subbands, respectively. M_S is saturation magnetization, M_Z - projection of the spatial magnetization vectors on z axis, where z is a quantization axis along the electron transport direction. **b** The tilting of the M_Z/M_S depending on the longitudinal cross section of the NW in form of the square with diameter d_0 , where A and B cases correspond to the constrained DW approach (here tilting is the same), C is the unconstrained case, $t_{\text{DW}} = t_0$, where the tilting is changed due to increased d_0

(out of the PC's center), but still the model will be valid due to the proximity of the systems. The lateral dimension t_{PC} of the PC, along z axis, is assumed to be vanishing. The contact plane is keeping validity of the quantum boundary conditions for an electron transport^{15; 22}. The segment's resistance of the NW can be estimated roughly *via* classical equation $R_{\text{Seg}} = 4\rho L_{\text{Seg}}/(\pi d_0^2)$, where ρ is the resistivity of the material at low dimension, L_{Seg} is a segment length. The total resistance of the system is $R_{\text{tot}} = R_{\text{Seg1}} + R_{\text{Seg2}} + R_{\text{PC}}$. The considered ΔR is the difference between R_{tot} with DW, where $R_{\text{PC}} \equiv R_{\text{DW}}$, and R_{tot} without one, where $R_{\text{PC}} \equiv R_0$, *i.e.* $\Delta R = R_{\text{DW}} - R_0$, where resistances from segments cancel each other. As a result, it is not necessary to consider the resistance of NW itself, the main focus of the present study is $R_{\text{PC}} = V/I_{\text{PC}}$ which have to be derived with and without DW. According to Useinov-Tagirov model¹⁵, the total charge current $I_{\text{PC}} = I_{\uparrow} + I_{\downarrow}$ is:

$$I_{\text{PC}} = \frac{2e^2}{h} \frac{AV}{2\pi} \sum_{s=\uparrow, \downarrow} k_{\text{F min},s}^2 \int_0^{\infty} dk \frac{J_1^2(ka)}{k} F_s(k) \quad (1)$$

where $J_1(ka)$ is Bessel function; the voltage-dependent transport term $F_s(k) = \langle \cos(\theta_{L,s}) D_s \rangle - N_{1,s}(k) \langle \cos(\theta_{L,s}) W_{L,s}(k) \rangle - N_{2,s}(k) \langle \cos(\theta_{L,s}) W_{R,s}(k) \rangle$ contains a ballistic ($d \ll \ell_s$) and diffusive-responsible ($d \gg \ell_s$) terms; The corner brack-

ets are averaging over incident angle of the electron trajectory $\theta_{L,s}$. In present model the possible quantization of the $\theta_{L,s}$ at the small dimensions is neglected for simplicity. Last two terms are responsible for diffusive and quasi-ballistic transport, they are sensitive to the spin-resolved MFP of electrons ℓ_s , they include integrals $N_{1(2)}$ and $W_{L(R)}$, which contain quantum mechanical transmission coefficient (QTC) of the system $D_s = D_s(\theta_{L,s}, V, k_s^L, k_s^R, d)$ and radial variable k ; Other parameters: $A = \frac{1}{4}\pi d^2$ is cross-section area of the PC, having a radius $a = \frac{1}{2}d$, $k_{\text{F min},s}$ is minimal spin-dependent Fermi wavenumber among k_s^L and k_s^R of the left (right) sides of the PC, s is a spin index. The assumption $D_s(\theta_{L,s}, V, k_s^L, k_s^R, d) \rightarrow D_s(\theta_{L,s}, V \rightarrow 0, k_s^L, k_s^R, d)$ is taken as reasonable for the DW simulation at the small positive voltage V , left side of NW (PC) is grounded. According to Bruno¹⁷, the unconstrained DW width threshold is $t_0 = 2\sqrt{A_{\text{ex}}/K_{\text{un}}}$, where A_{ex} and K_{un} are exchange stiffness constant and uniaxial magnetocrystalline anisotropy constant in metal. For example, it gives $t_0 = 10.6$ nm at $A_{\text{ex}} = 1.4 \times 10^{-6}$ erg/cm and $K_{\text{un}} = 5.0 \times 10^6$ erg/cm³ for Co NW, borrowing material parameters from Ebels *et al.*²³. Applying these estimations, the condition of the constrained DW is used as a main approach, here $t_{\text{DW}} = d$ at $t_{\text{DW}} < t_0$. Another words, t_{DW} is a varying parameter of the system, which approximately grows

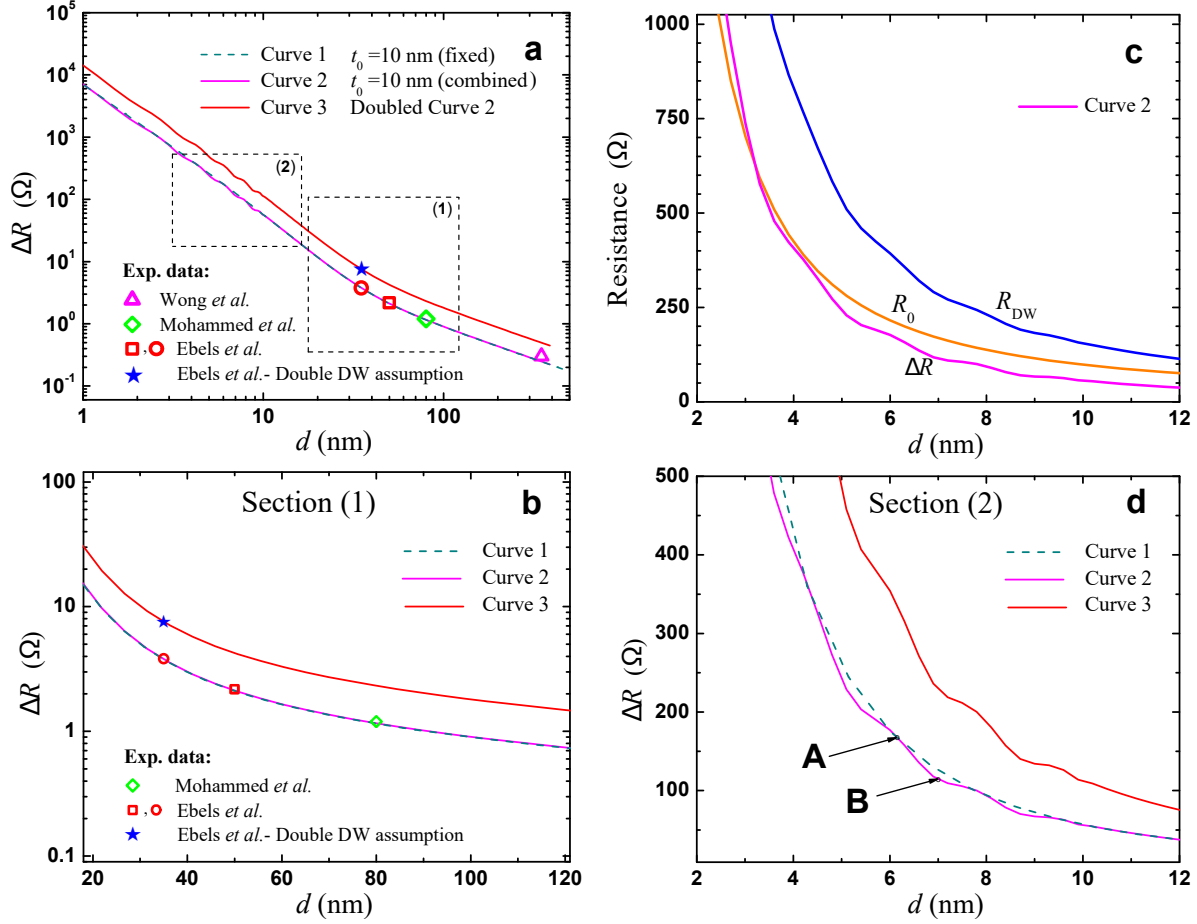


Fig. 2. Domain wall resistance ΔR vs. diameter of the PC, $d \rightarrow d_0$. **a** Curves 1 and 2 correspond to the cases of the ΔR at fixed $t_{\text{DW}} = t_0 = 10$ nm, and the one for the combined case: $t_{\text{DW}} = d$, while $t_{\text{DW}} = t_0$, at $d > t_0$, highlighting ΔR oscillations with d and how the curves are matched with experimental data. Curve 3 shows the doubled DW resistance $2\Delta R$ with d . Other parameters are common for these curves: $\ell_{\uparrow}^{L(R)} = 12$ nm, $\ell_{\downarrow}^{L(R)} = 3.0$ nm; $k_{\uparrow}^L = 0.61 \text{ \AA}^{-1}$, $k_{\downarrow}^L = 1.08 \text{ \AA}^{-1}$, $k_{\downarrow}^R = 1.0801 \text{ \AA}^{-1}$ and $k_{\uparrow}^R = 0.6101 \text{ \AA}^{-1}$. Panel **c** shows R_{DW} and R_0 and resulting $\Delta R = R_{\text{DW}} - R_0$ at linear scale, where the oscillations are most visible. Panels **b** and **d** show a zoom of sections (1) and (2), respectively. **d** Two points A and B demonstrate the relative 10% deviation of the curves 1 and 2 from each other.

up with d until t_0 is achieved. The condition when d is comparable with one of the spin-dependent MFP is important for the considered ΔR behavior. The wide range of t_0 is theoretically considered here: $t_0 = 10$ nm, $t_0 = 16$ nm and $t_0 = 36$ nm. Since the spin diffusion length is around 60 nm in Co, that is large enough than t_0 , an impact of the electron spin flip leakages is out of present consideration. The exact analytical solution for the spin-dependent QTC, which is based on Airy functions for the sloped potential and available in Ref.¹⁴, was used for the tail-removed DW, characterizing the electron scattering from ballistic to diffusive conditions. The considered QTC is applicable for

two spin channels with D_{\uparrow} and D_{\downarrow} , while the case without DW corresponds to the condition when $D_{\uparrow(\downarrow)} = 1.0$. The approach of small V in the model of the symmetric (homogeneous) NW assumes that k_s^R are taken as voltage independent, but slightly larger than k_s^L for the negligibly small positive V . In contrast, segmented NWs with periodical Co/Ni interfaces naturally have initially different k_s^L and k_s^R values. As a result of fitting with an experimental data in the section below, the following initial k_s and l_s are found for Co NW: $k_{\uparrow}^L = 0.61 \text{ \AA}^{-1}$, $k_{\uparrow}^R = 0.6101 \text{ \AA}^{-1}$, $k_{\downarrow}^L = 1.08 \text{ \AA}^{-1}$, $k_{\downarrow}^R = 1.0801 \text{ \AA}^{-1}$, and $\ell_{\uparrow}^{L(R)} = 12.0$ nm, $\ell_{\downarrow}^{L(R)} = 3.0$ nm, however, ℓ_{\downarrow}^L

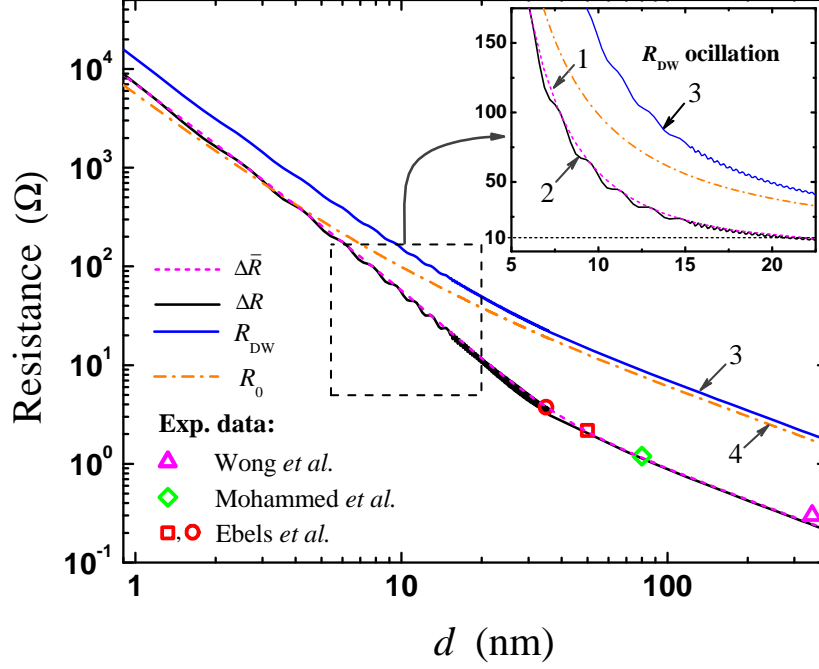


Fig. 3. Single DW resistance *vs.* diameter of the PC, that approximately equals to the DW resistance in NW at the condition $d \rightarrow d_0$. Curves 1 correspond to the case of the $\Delta\bar{R}$ at $t_{\text{DW}} = t_0 = 10$ nm, and curve 2, $\Delta R = R_{\text{DW}} - R_0$, is derived for the combined case of the DW width: $t_{\text{DW}}(d > t_0) = 36.0$ nm, while $t_{\text{DW}}(d \leq t_0) = d$, $t_0 = 36$ nm. Curves 3 and 4 show the resistance of the PC with and without DW for the combined case, respectively. Other parameters are the same as in Fig.2. The inset shows a zoom of the resistance oscillation of the single DW in linear scale.

was changed to $\ell_{\downarrow}^L = 4.0$ nm for a better matching for the segmented Co/Ni NW, that, probably, related with a different lattice properties in relation to uniform Co NW. The conduction band spin polarization parameter $\delta_{\text{Co}} = k_{\uparrow}/k_{\downarrow}$ is equal to 0.56, that numerically coincides with the one in Ref. ²⁴, noting that simulations in present work give the same results making the complete spin index reversal \downarrow (\uparrow) to \uparrow (\downarrow) for each material parameter. The additional sources of experimental estimations of the spin-resolved Fermi wavenumbers and theoretical simulations of the averaged ℓ in different metals are available in Ref. ²⁵ and Ref. ²⁶, respectively.

3. Results and Discussions

The result of calculations for the DW resistance behaviors are shown in Fig.2, $t_0 = 10$ nm. There are two cases for the fixed ($t_{\text{DW}}(d) = t_0$ at any d , see curve 1) and combined DW width dependencies ($t_{\text{DW}}(d) = d$ at $d \leq t_0$ while $t_{\text{DW}}(d) = t_0$ at $d > t_0$ for curve 2), respectively. Theoretical curves, considered for comparison with each other and experimental data, are shown in Fig.2a and Fig.2b. Experimental points are obtained as $\Delta R = 0.3 \Omega$ at

$d_0 = 300$ nm for Permalloy (Py) $\text{Ni}_{80}\text{Fe}_{20}$ NWs according Wong *et al.*¹⁹; $\Delta R = 1.2 \Omega$ at $d_0 = 80$ nm by Mohammed *et al.*^{5; 6} for Co/Ni segmented NW; $\Delta R = 2.178 \Omega$ at $d_0 = 50$ nm, and finally, $\Delta R = 7.5 \Omega$ at $d_0 = 35$ nm for uniform Co NWs by Ebels *et al.*²³. The last point for $d_0 = 35$ nm is considered as a result of two DW's contributions, since a single DW resistance at this dimension is expected to be a half of 7.5Ω , *i.e.* $\Delta R = 3.75 \Omega$, noting that Ebels *et al.* also assumed the presence of the doubled DW at this point. In case of a few DWs, existing in NW, the related DW resistance is a few times higher, respectively. Two points A and B in Fig.2d demonstrate the relative 10% deviation of the curves 1 and 2 from each other due to the oscillation of the curve 2. These deviations are suppressed at $t_{\text{DW}}(d) > 10$ nm and raised due to presence of the DW at the confined geometry of PC, *e.g.* Fig.2c clearly shows the related R_{DW} oscillations with d .

The calculated $\Delta\bar{R}(d)$ and $\Delta R(d)$ - curves 1 and 2 for the fixed t_{DW} and combined cases are also shown in Fig.3, their minor difference due to logarithmic scale is more clearly highlighted in the in-

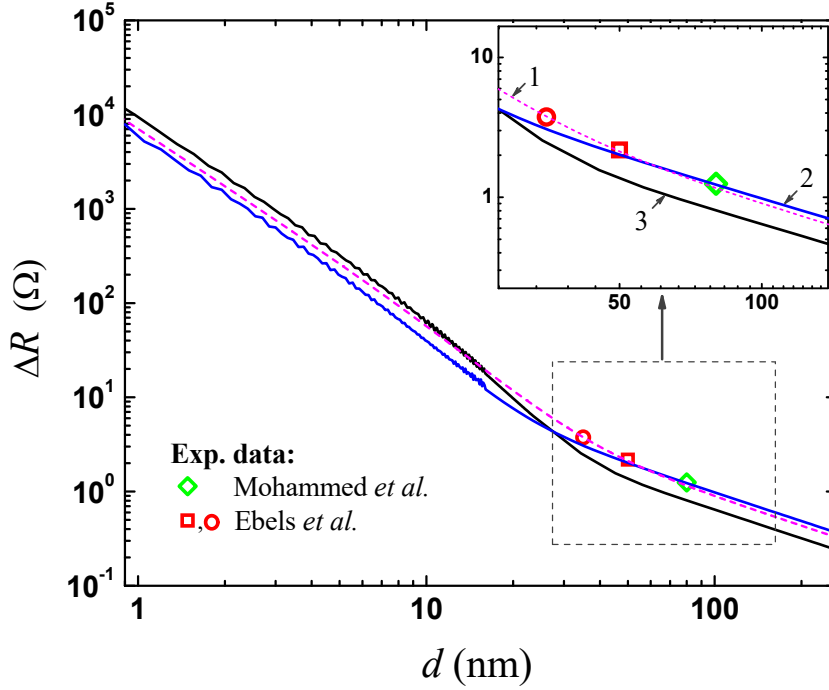


Fig. 4. Single DW resistance *vs.* diameter of the asymmetric PC, corresponding to the DW resistance in segmented NWs at $d \rightarrow d_0$. Parameters for the curve 2 is oriented for Co/Ni interface: $t_0 = 16$ nm, $k_{\uparrow}^L = 0.61$ Å⁻¹, $k_{\downarrow}^L = 1.08$ Å⁻¹, $k_{\uparrow}^R = 0.65$ Å⁻¹, $k_{\downarrow}^R = 1.0801$ Å⁻¹, $\ell_{\uparrow}^L = 12.0$ nm, $\ell_{\downarrow}^L = 4.0$ nm, $\ell_{\uparrow}^R = 6.0$ nm, $\ell_{\downarrow}^R = 1.5$ nm, having $\ell_{\uparrow}^L/\ell_{\downarrow}^L = 3.0$ and $\ell_{\uparrow}^R/\ell_{\downarrow}^R = 4.0$; Parameters for the curve 3: t_0 , k_{\downarrow}^L , k_{\uparrow}^R , k_{\downarrow}^R , ℓ_{\uparrow}^L and ℓ_{\downarrow}^L are the same as for the curve 2, while $k_{\uparrow}^L = 0.41$ Å⁻¹, $\ell_{\uparrow}^R = 5.8$ nm, $\ell_{\downarrow}^R = 1.95$ nm and $\ell_{\uparrow}^{L(R)}/\ell_{\downarrow}^{L(R)} = 3.0$. Dashed curve 1 is symmetric case of the Co-based PC, that coincides with curve 1 in Fig.3.

set with liner scale. The black curve 2 is calculated in such a way to consider possible large value of $t_0 = 36.0$ nm to see the condition, where oscillations will be over. Figure 3 includes the curves for PC's resistances with presence of the DW R_{DW} - blue curve 3, and without R_0 - orange dash-dotted curve 4, correlating with the given behavior of the curve 2. It is obvious, that the reason of the ΔR oscillations is R_{DW} variations. Its origin is the MFP dimensional effects due to ballistic and quasi-ballistic conditions of the electron scattering, where related barrier transparency *vs.* t_{DW} behave dissimilar in relation to clear ballistic, or diffusive conditions. The most obvious range of the step-like oscillations is $\Delta R \approx 10 \Omega - 300 \Omega$ at around $d \approx 2.5$ nm–16.0 nm, that is comparable with the range between minimal $\ell_{\min} = \ell_{\downarrow}$ and maximal $\ell_{\max} = \ell_{\uparrow}$ values. In particular, for the case $\ell_{\min} < t_{DW} < \ell_{\max}$, the electron scattering on the DW is intermixed by two conductive spin channels at two different conditions: ballistic for electrons with spin up, while quasi-ballistic condition takes place for electrons spin down. The amplitude of oscillation is proportional to the dif-

ference between ℓ_{\max} and ℓ_{\min} . It should be noticed that observed ΔR steps can be used in fabrication for the minimization of the NW size distribution influence on a dispersion of the total resistance in NWs arrays, *e.g.* the convenient range of the stable ΔR value is $d \approx 10.4$ nm–11.2 nm, where $\Delta R = 45.1 \Omega$ which the third step from the left side of the inset, Fig.3. The oscillation averaged period is almost a constant value, that is around 1.73 nm at $d = 2.1$ nm–15.2 nm, while the range $d = 15.2$ nm–36.0 nm ($d \approx 1.5\ell_{\max} - 3\ell_{\max}$) is different since the transport is more diffusive: the period of the oscillations monotonically decreases with a suppressed amplitude here. An important sensitive parameter for the system is the MFP ratio $\ell_{\uparrow}^{L(R)}/\ell_{\downarrow}^{L(R)}$. For the curves in Fig.3, it is fixed for simplicity as $\ell_{\uparrow}^{L(R)}/\ell_{\downarrow}^{L(R)} = 4.0$, being oriented mainly for homogeneous Co NW, rather than for the Py and Co/Ni cases. The estimation of the giant BMR, which can be determined as $BMR = (R_{DW} - R_0)/R_0 \cdot 100\%$, gives 124% for $d = 1.2$ nm. The point at $d = 350$ nm for Py NW is nicely fitted

by $\ell_{\uparrow}^{L(R)}/\ell_{\downarrow}^{L(R)} = 4.5$ (not shown), while the point $d = 80$ nm for Co/Ni NW is more precisely fitted by segmented NW's model, described below.

In addition to the homogeneous case, it is worth to consider segmented NW (or asymmetric PC), where spin-resolved k_s and ℓ_s values are different for the left and right sides of the interface between segments. It was found that the oscillation of ΔR also take place in this case for a constrained DW, however, its amplitude are much less in relation to homogeneous one, and its period is not monotonic, Fig.4. The asymmetry is divided on two cases: the first when the curve 2 shows ΔR for the both asymmetries by $k_{\uparrow}/k_{\downarrow}$ and $\ell_{\uparrow}/\ell_{\downarrow}$ ratios in the left and right sides, and second case when the curve 3 corresponds to the asymmetry by the $k_{\uparrow}/k_{\downarrow}$ ratio only. In contrast to curve 2, curve 3 has larger difference between k_{\uparrow}^L and k_{\downarrow}^L , its $\Delta R(d)$ is higher in the ballistic range and lower in the diffusive one. Moreover, there are diameters at the ballistic range for the curve 3, at which ΔR oscillations are suppressed, that is not well observed for the curve 2. The blue curve 2 in the diffusive regime with $\ell_{\uparrow}^L/\ell_{\downarrow}^L = 3.0$ and $\ell_{\uparrow}^R/\ell_{\downarrow}^R = 4.0$ better fits experimental point for the Co/Ni segmented NW at $d_0 = 80$ nm (green rhombus) than the case of homogeneous Co NW $\ell_{\uparrow}^{L(R)}/\ell_{\downarrow}^{L(R)} = 4.0$ (curve 1), see the inset in Fig.4. As a result, curve 2 and curve 3, representing asymmetric cases, additionally proof that ℓ_s ratios are the most valuable parameters in $\Delta R(d)$ behavior. This property can be used, for example, in simulation and fabrication of the magnetic interconnects, DW memory, *etc*, decreasing unwanted resistance dispersion. Raw data and program code are available online ²⁷.

4. Conclusion

The adapted point-like contact model allows successfully describe experimental data of the single and double DW resistances in magnetic junctions and cylindrical NWs, when diameters of the NW and PC are close values. Almost four orders ΔR drop is held within only two orders by d , *e.g* theory predicts 7 k Ω for $d \approx 1$ nm and 0.88 Ω for $d \approx 100$ nm. The system is sensitive to the ratios of the spin-resolved electron MFP and wavenumbers of the magnetic material. The reason of the found ΔR oscillations with d is the flexible DW approach when $d = t_{\text{DW}}$ and take place the case of $l_{\text{min}} < t_{\text{DW}} < l_{\text{max}}$ at which electron scattering on the DW has intermixing conditions: ballistic for one electron spin

orientation and quasi-ballistic for another. The presented ΔR oscillations for Co nanowire, where the relative amplitude of oscillations does not exceed 10%, are not related to quantization phenomena, or tilting of the DW-induced potential at $t_{\text{DW}} > t_0$, amplitude of oscillations vanishes when the system approaches $t_{\text{DW}} > 1.25 l_{\text{max}}$ and competition between ballistic and quasi-ballistic regimes is over. The ΔR steps can be used for the minimization of the total resistance dispersion coming from the size distribution of a large amount of NWs, it may help to detect approximate NW's dimension measuring only its resistance with and without DW, and support a further development of the racetrack memory concept.

Data Availability

The raw data and program code: <https://data.mendeley.com/datasets/kmsjt7kndk/1>.

Acknowledgment

This work was financially supported by the "Center for the Semiconductor Technology Research" from The Featured Areas Research Center Program within the framework of the Higher Education Sprout Project by the Ministry of Education (MOE) in Taiwan. Also supported in part by the Ministry of Science and Technology, Taiwan, under Grant MOST 110-2634-F-009-027- and MOST 110-2112-M-A49-016-

References

1. D. A. Allwood, G. Xiong, C. C. Faulkner, *et al.* Magnetic domain-wall logic, *Science* **309** 1688 (2005).
2. S. Lequeux *et al.*, A magnetic synapse: multilevel spin-torque memristor with perpendicular anisotropy, *Sci. Rep.* **6** 31510 (2016).
3. D. Kaushik, U. Singh, U. Sahu, I. Sreedevi, and D. Bhowmik, Comparing domain wall synapse with other non volatile memory devices for on-chip learning in analog hardware neural network, *AIP Adv.* **10** 025111 (2020).
4. S. S. P. Parkin, M. Hayashi, and L. Thomas, Magnetic domain-wall racetrack memory, *Science* **320** 190 (2008).
5. H. Mohammed, H. Corte-León, Y. P. Ivanov, *et al.* Current controlled magnetization switching in cylindrical nanowires for high-density 3D memory applications, <https://arxiv.org/pdf/1804.06616v1>
6. H. Mohammed, H. Corte-León, Y. P. Ivanov, *et al.* Angular magnetoresistance of nanowires with al-

- ternating cobalt and nickel segments, *IEEE Trans. Magn.* **53** 1–5 (2017).
7. M. Chandra Sekhar, S. Goolaup, I. Purnama, and W. S. Lew, Depinning assisted by domain wall deformation in cylindrical NiFe nanowires, *J. App. Phys.* **115** 083913 (2014).
 8. H.-G. Piao, J.-H. Shim, D. Djuhana, and D.-H. Kim, Intrinsic pinning behavior and propagation onset of three-dimensional Bloch-point domain wall in a cylindrical ferromagnetic nanowire, *Appl. Phys. Lett.* **102** 112405 (2013).
 9. M. Yan, A. Kákay, S. Gliga, and R. Hertel, Beating the Walker limit with nassless domain walls in cylindrical nanowires, *Phys. Rev. Lett.* **104** 057201 (2010).
 10. P. M. Levy and S. Zhang, Resistivity due to domain wall scattering, *Phys. Rev. Lett.* **79** 5110–5113 (1997).
 11. G. Tatara and H. Fukuyama, Resistivity due to a Domain Wall in Ferromagnetic Metal, *Phys. Rev. Lett.* **78** 3773–3776 (1997).
 12. G. Tatara and N. García, Theory of domain wall resistance in nanocontacts, *IEEE Trans. Magn.* **36** 2839–2840 (2000).
 13. C. Hassel, M. Brands, F. Y. Lo, *et al.*, Resistance of a single domain wall in (Co/Pt)₇ multilayer nanowires, *Phys. Rev. Lett.* **97** 226805 (2006).
 14. A. N. Useinov, R. G. Deminov, L. R. Tagirov, G. Pan, Giant magnetoresistance in nanoscale ferromagnetic heterocontacts, *J. Phys.: Condens. Matter* **19** 196215 (2007).
 15. A. Useinov, H.-H. Lin, N. Useinov, and L. Tagirov, Spin-resolved electron transport in nanoscale heterojunctions. Theory and applications, *J. Magn. Magn. Mater.* **508** 166729 (2020).
 16. N. García, M. Muñoz, and Y.-W. Zhao, Magnetoresistance in excess of 200% in ballistic Ni nanocontacts at room temperature and 100 Oe, *Phys. Rev. Lett.* **82** 2923–2926 (1999).
 17. P. Bruno, Geometrically constrained magnetic wall, *Phys. Rev. Lett.* **83** 2425–2428 (1999).
 18. S. Da Col *et al.*, Observation of Bloch-point domain walls in cylindrical magnetic nanowires, *Phys. Rev. B* **89** 180405 (2014).
 19. D. W. Wong, I. Purnama, G. J. Lim, *et al.* Current-induced three-dimensional domain wall propagation in cylindrical NiFe nanowires, *J. App. Phys.* **119** 153902 (2016).
 20. R. Wieser, U. Nowak, and K. D. Usadel, Domain wall mobility in nanowires: Transverse versus vortex walls, *Phys. Rev. B* **69** 064401 (2004).
 21. A. N. Useinov, L. R. Tagirov, R. G. Deminov, Y. Zhou, and G. Pan, Mean-free path effects in magnetoresistance of ferromagnetic nanocontacts, *Eur. Phys. J. B* **60** 187–192 (2007).
 22. A. Useinov, H.-H. Lin, N. Useinov, and L. Tagirov, Mathematical description data: Spin-resolved electron transport in nanoscale heterojunctions: Theory and applications, *Data in Brief* **32** 106233 (2020).
 23. U. Ebels, A. Radulescu, Y. Henry, L. Piraux, and K. Ounadjela, Spin accumulation and domain wall magnetoresistance in 35 nm Co wires, *Phys. Rev. Lett.* **84** 983–986 (2000).
 24. L. R. Tagirov and N. García, Quasiclassical boundary conditions for a contact of two metals, *Superlattice. Microst.* **41** 152–162 (2007).
 25. F. J. Himpsel, K. N. Altmann, G. J. Mankey, *et al.* Electronic states in magnetic nanostructures, *J. Magn. Magn. Mater.* **200** 456–469 (1999).
 26. D. Gall, Electron mean free path in elemental metals, *J. App. Phys.* **119** 085101 (2016).
 27. <https://data.mendeley.com/datasets/kmsjt7kndk/1>